Netsu Sokutei **43** (3), 105-112 (2016)

Review

Investigating with *P,V,T*-Calorimetry the Large Surface Energies Developed by Lyophobic Porous Solids upon Intrusion/Extrusion of Non-Wetting Liquids*

Yaroslav Grosu and Jean-Pierre E. Grolier

University Clermont Auvergne, ENSCCF, Institute of Chemistry of Clermont-Ferrand
CNRS, UMR 6296 63177 Aubière, France

(Received Feb. 25, 2016; Accepted Apr.4, 2016)

Large surface energy can be developed using highly porous Heterogeneous Lyophobic Systems (HLSs) which comprise a mesoporous solid and a non-wetting liquid to make working bodies. Such systems exhibit remarkable properties and characteristics such as high energy capacity, capability to simultaneously store (and restore) both thermal and mechanical energy during intrusion/extrusion of the liquid during compression/decompression operations. Usually an HLS is in the form of a suspension of a porous powder in the liquid. We have developed a *P,V,T*-calorimetry-volumetry system which can judicially be used to submit such suspension to compression/ decompression in a perfectly controlled thermodynamic way over extended *T*- and *P*-ranges. As a matter of fact, depending on the nature of the porous solid and of the non-wetting liquid it is always possible to find a high enough pressure to force the intrusion by compression of the liquid in the pores of the solid. The compression energy being store in the system can be further restored. We show how easily we can obtain the thermal and mechanical energies generated during repeated compression/decompression cycles while recording the associated *P,V*- diagrams.

Keywords: *PVT*-calorimetry, high pressure, interface energy, liquid intrusion-extrusion, porous solids

Yaroslav Grosu

Jean-Pierre E. Grolier
E-mail: j-pierre.grolier@univ-bpclermont.fr

*This paper was communicated in part by Jean-Pierre E. Grolier as a Plenary Lecture at the 51rst Japanese Conference on Calorimetry and Thermal Analysis (51rst JCCTA) in Kawanoge, Japan, 8-10 October 2015.
It is dedicated to the Memory of Professor Valentine A. Eroshenko, National Technical University of Ukraine, "Kyiv Polytechnic Institute"

1. Introduction

In the active search for a new source of energy which includes its rational utilization and storage, surface energy (a 2D energy) appears now as a challenging option thanks to new available porous materials of all sorts. Large surface energy can be developed using highly porous Heterogeneous Lyophobic Systems (HLSs) which comprise a mesoporous solid and a non-wetting liquid to make remarkable working bodies.

Methods of forced intrusion of a non-wetting liquid (such as mercury or water porosimetry) are widely used for porous materials characterization in such fields as catalysis, chromatography, adsorption, pharmaceutical and petroleum science [1,2] and are still under improvement.[3] High-pressure water intrusion–extrusion cycles constitute the usual operational cycles for {porous materials + a non-wetting liquid} systems to accumulate mechanical and thermal energy by means of forced intrusion of the liquid into the pores.

The non-wetting condition eliminates the spontaneous penetration of the liquid into the pores of the matrix. By increasing the pressure of the system to some critical value (intrusion pressure P_{int}) the liquid can be forced into the pores; the mechanical energy necessary to break the intermolecular bonds of the liquid during intrusion is supplied to the system during the intrusion process and is associated with the "solid–liquid" interface development. On the *PV*-diagram this process corresponds to an intrusion plateau and is associated to a significant increase of the compressibility of the system (**Fig.1**): the corresponding plateau stands until the pores of the matrix are completely filled. Since lyophobic pores constitute an energetically unfavorable environment for molecules of the non-wetting liquid, the decrease of the pressure in the system down to some critical value (extrusion pressure P_{ext}) leads to the extrusion of the liquid from the pores of the matrix, which is followed by the release of mechanical energy (large expansion of the system, see **Fig.1**) and renewal of intermolecular bonds of the liquid. Hence, such HLS system acts as a molecular spring (MS) and can be used for energy storage. [4-7]

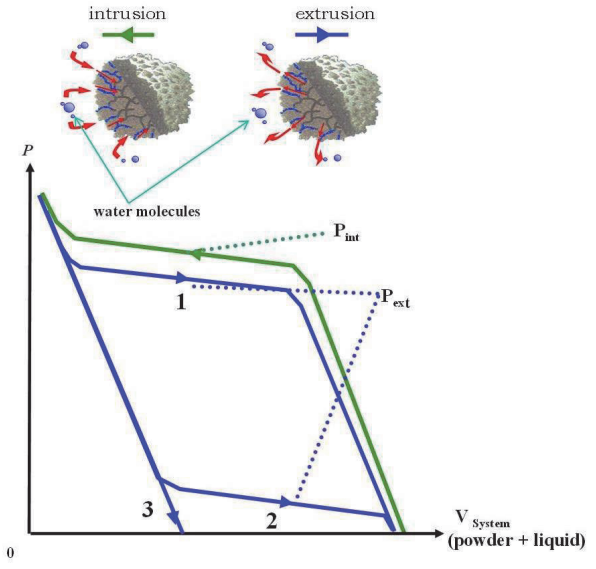

Fig.1 Isothermal *PV*-diagram showing intrusion pressure P_{int} (along the intrusion plateau) and extrusion P_{ext} of water molecules in/out grains of a porous material. Three possible extrusion situations after initial intrusion are illustrated, depending on the hysteresis $H = [P_{int} - P_{ext}] / P_{int}$: 1) $P_{int} \sim P_{ext}$, $H = 0$, reversibility; 2) $P_{int} >> P_{ext}$, $H = 0.95$, energy dissipation; 3) no extrusion, $H \sim 1$.

In particular, the process of reversible intrusion of water into hydrophobic porous media forms the basis for molecular springs operation [such heterogeneous lyophobic systems being also called repulsive clathrates [8] RCs]; [4,5,9-12] while novel high efficient shock-absorbers based on heterogeneous lyophobic systems (HLSs) take advantage of liquid intrusion irreversibility. [6,13-20].

During the intrusion process the system consisting of a lyophobic porous matrix and a non-wetting liquid stores over the interface Ω development $(d\Omega > 0)$ mechanical energy in the form of Gibbs work $(\delta W^{\Omega} = \sigma cos\theta d\Omega)$ and thermal energy in the form of heat of interface Ω development $\left(\delta Q^{\Omega} = T\frac{d\sigma cos\theta}{dT}d\Omega\right)$. The system restores these energies as a result of the interface reduction during the extrusion process $(d\Omega < 0)$; $\theta > 90°$ is the contact angle, σ is the surface tension of the liquid, T is temperature. If this process is close to reversible (situation "1" in **Fig.1**), the system acts as a molecular spring (MS),[4,21-24] if not it behaves (situations "2" and "3"in **Fig.1**) as a shock-absorber or a bumper.[25-27] The major interest in investigating MSs is due to their energy capacity, orders of magnitude higher in comparison with conventional working bodies,[4,24-26] which is reached by using lyophobic porous materials with large values of specific surface Ω. Recently the range of porous matrices for MSs has been extended to metal-organic frameworks (MOFs).[25] MOFs are of great interest due to their exceptional stability and large porosity, which are well suited in many fields of science and technology.[27,28] The specific energy which the MOF system stores/restores during the intrusion/extrusion process can be obtained by using porous materials with a large specific surface area ($400 - 2000\ m^2\ g^{-1}$) possessing a large specific volume change (able to generate mechanical energy) during intrusion/extrusion processes.

The pronounced porosity and high stability of Metal Organic Frameworks (MOFs) and particularly their subclass of Zeolitic Imidazolate Frameworks (ZIFs) attract increasing attention in many fields of science and technology.[28] Applications include gas separation [29], catalysis, [30] drug delivery,[31] mechanical energy storage (taking advantage of their reversible high flexibility [32] or of non-wetting liquid intrusion–extrusion[7,25,33,34]), and systems with negative thermal expansion.[35] As a matter of fact, ZIFs are particularly interesting due to their exceptional stability, which is essential for practical applications. For all these applications in-depth understanding of the stability conditions of MOFs is obviously very important.

Indeed, it has been shown both by experiments [36-39] and by simulations [40,41] that even for the most "fragile" ZIFs rather high values of pressure and temperature are required to generate irreversible structural changes: for example for ZIF-8 the critical (hydrostatic and non-hydrostatic) pressure after which irreversible amorphisation takes place is ~0.34 GPa according to Chapman *et al.*[36] or even 1.6 GPa according to Hu *et al.* (non-hydrostatic), [42] while for ZIF-4 it is ~6.5 GPa.[38] Naturally most of the studies on the stability of ZIFs characteristics were implemented to investigate separately the effects of pressure and temperature on the structure of the materials. However, no studies have been devoted to the concomitant effects of pressure and temperature on the structures of ZIFs. High pressure compression–decompression cycles over a wide temperature range are typical operational conditions for porous heterogeneous lyophobic systems (HLSs) used for energy storage, transformation or dissipation (depending on the type of HLS). [4,17,18,21] Recently the class of porous materials for HLS was extended to hydrophobic ZIF-8 [25,33,43] and ZIF-71 [34] metal organic frameworks. Such ZIFs demonstrated excellent characteristics when forming HLSs combined with water [25,34,43] and aqueous electrolyte solutions. [25,33,34] However, the effect of

temperature on their characteristics was not investigated and for the first time we have undertaken high-pressure calorimetric investigations for the {ZIF-8 + water} system in the 275–360 K temperature range to document its characteristics in terms of thermal and mechanical energy storage.[42,43] In order to explore the combined effects of pressure and temperature on the structure of ZIF-8 (and hence on the stability of the {ZIF-8 + water system}) additional X-Ray Diffraction (XRD), Fourier Transform Infra-Red (FTIR) spectroscopy and Scanning Electron Microscopy (SEM) characterization (non reported here) have been performed before and after compression–decompression cycles of the {ZIF-8 + water} system.[44] Yet investigations under conditions other than at room temperature are still very rare in the literature.

2. Intrusion/Extrusion of a non-wetting Liquid in a lyophobic Porous Solid

2.1 Materials

In this review, as reported in ref.44 and 35, three porous heterogeneous lyophobic systems (HLSs) based on water were used. Hydrophobic porous materials are as follows, one silica gel and two metal organic frameworks (MOFs), hydrophobic microporous zeolitic imidazolate frameworks (ZIFs): (1) commercial mesoporous silica gel SymmetryPrep C8, in the shape of 7 μm granules grafted with octylsilanes with density of 2.1 groups/nm^2 according to the data provided by the supplier (WATERS). The average pore radius is 4.2 nm; the pore volume is 0.53 cm^3 g^{-1}; the HLS based on this matrix is referred to as {WC8 + water}. [35] (2) ZIF-8 purchased from Sigma-Aldrich as Basolite Z1200, the HLS based on this matrix is referred as {ZIF-8 + water}. (3) ZIF-67 ($Co(Hmim)_2$, Hmim 1/4 2-methylimidazole) was purchased from MOF Technologies. Particularly ZIF-67 and ZIF-8 have specific surfaces of 1500 m^2 g^{-1} and 1800 m^2 g^{-1} respectively. [45,46] Both materials have pore opening of only 3.4 Å and cages of 11.6 Å.[47] the HLS based on this matrix is referred as {ZIF-67 + water}. ZIF-67 is isostructural to ZIF-8, which has sodalite (SOD) topology and is formed by bridging 2-methylimidazolate anions and zinc cations. Distilled water was used as non-wetting liquid for both all investigated systems.

Recent experimental measurements demonstrate that original devices making use of selected HLSs can serve as working bodies to store/restore energy, with systems behaving like molecular springs or showing negative thermal expansion. In this sense MOFs with their large surfaces are attractive candidates for that matter. Testing ZIF-67 as a component of HLS with water and its stability upon water intrusion–extrusion at different temperatures follows successful tests of {ZIF-8 + water} [7,25] and {ZIF-71 + water}[34] systems for energy applications.

It is important to note that these systems were tested in slow (quasi static) operational regimes, while real applications may require much faster compression/decompression (intrusion/extrusion) cycling. For example it is worth to mention that a HLS based on grafted silica gels and water can sustain operational frequencies up to 22 Hz [16,19] and potentially much higher,[48] but to our knowledge the effect of compression/decompression speed on the characteristics of HLSs based on MOFs has never been documented. Here we report a first step in investigating such effect for {ZIF-67 + water} and {ZIF-8 + water} systems; in particular the effect of speed of compression/decompression and the framework relaxation time of these ZIFs are discussed.

2.2 Experimental

A ST-7M transitiometer (BGR-Tech) was used to obtain the *PV*-isotherms of the investigated systems in the 275–360 K temperature and 0.1–30 MPa pressure ranges at different speeds ranging from 0.01 MPa min^{-1} to 5.5 MPa min^{-1} according to the procedure described elsewhere.[12] The ST-7M transitiometer is a modified version of the ST-7 instrument (BGR-Tech) [50]; it was used to obtain the *PV*-isotherms and thermal effects of the HLSs along compression-decompression cycles. In contrast to the conventional ST-7, [50-53] metal bellows connected to high-precision induction volumeters were soldered to the high-pressure transitiometric vessels (for pressure up to 200 MPa) of the ST-7M.

The experimental setup is shown in **Fig.2**. The opened upper ends of bellows are soldered to the bottoms of the cylindrical part of the transitiometric vessels. The investigated sample is placed inside a special metallic capsule inserted in the measuring vessel while a reference sample is similarly seating in the reference vessel. The bottoms of bellows are connected through non-magnetic metal rods to the magnetic core of the induction sensors for the linear variable differential transformer (LVDT) detection. The active parts of induction sensors are located in chambers made of non-magnetic material which are outside of the calorimeter detecting zone. The changes in volume during the compression-decompression of the HLSs are directly obtained from the axial displacement of the bellows' bottoms; the

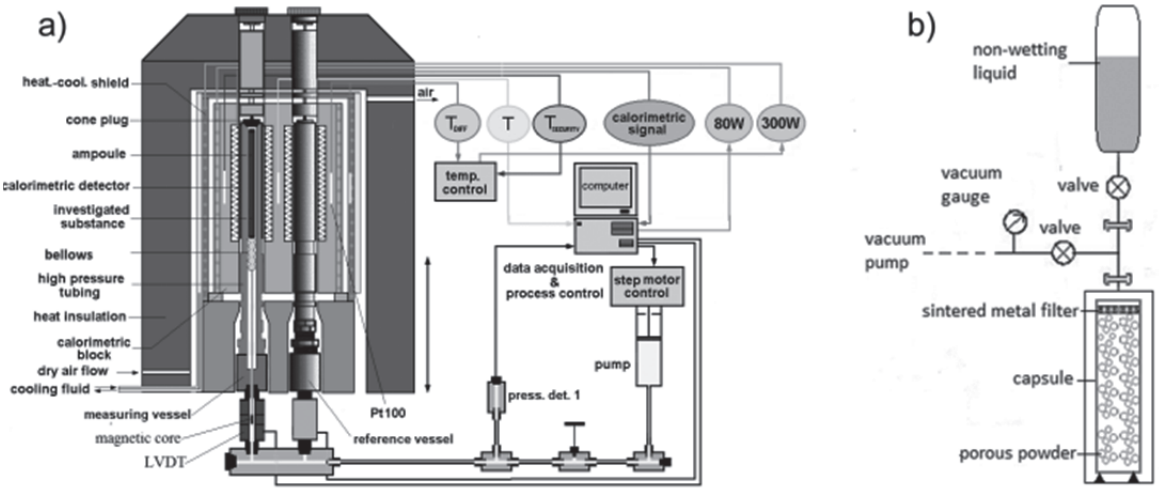

Fig.2 a) The experimental setup for determining the *PV*-diagram and associated heat effects. The measuring vessel on the left hand side shows the bellows connected to the high pressure line through the magnetic core device for the LVDT detection. b) The setup used for degassing and filling the heterogeneous sample into the metallic capsule closed with a sintered metal filter.

displacement is detected by the LVDT differential transformer device.[54] Reading of the LVDT signals, calibrated in terms of volume, can be activated both in parallel and differentially. The pressure in the measuring cell is generated by a high-pressure (HP) pump, driven by a stepping motor. Changes in the system's volume are then registered by the induction volumeters through the LVDT devices. Recording of pressure in the hydraulic system is made via a pressure sensor (see press.det.1 in **Fig.2**) built in the hydraulic line connecting the pump to the transitiometric vessels (see **Fig.2**).

The instrument can be operated in different modes [49-53] via its complete control by Lab View programming. Changes in the volume of the investigated system, the pressure increase and the differential heat flow between the measuring and reference vessels during pressure scans are simultaneously recorded (by computer) at a constant temperature (within ±1 mW sensitivity). The rate of volumetric changes is approximately 10^{-4} cm^3 s^{-1}, since low scanning speed is compulsory to ensure thermal equilibrium and to minimize thermal gradients during the scanning process. Measurements are performed in controlling precisely the three thermodynamic variables, namely: for pressure within ± 0.15 MPa, for volume within ± 3.3・10^{-4} cm^3 and at constant temperature within ± 0.01 K.

The simplified scheme of sample preparation is illustrated in **Fig.2(b)**. A specific amount of MOF is introduced into the metallic capsule, which is sealed by a metallic-ceramic porous cover. An approximate weight (~ 0.5 g) of the porous powder is inserted in the capsule. The capsule with powder is thoroughly degassed to about 10^{-2} mbar for 2-4 hours. After the degassing procedure, the capsule with powder is filled *in situ* under vacuum with degassed distilled water through the porous cover. This procedure guarantees efficient filling of interparticle spaces by water. The {MOF + water} system constitutes the investigated HLS. The capsule containing the HLS is positioned in the measuring vessel while an identical capsule just filled with degassed water is positioned in the reference vessel; both vessels are initially filled with degassed water. During immersion of capsules inside the calorimetric vessels the water in excess is freely forced out from the cells through small outlets which block air from entering cells. These outlets are then tightly sealed by special screw caps and the calorimetric detector with two receiving thermopiles is gently lowered over both vessels. Tight fit of the vessels in the calorimetric thermopiles within the calorimetric detector provides the efficient heat transfer between measuring and reference vessels with the corresponding thermopiles. This arrangement allows measuring the differential heat flux between the two vessels, yielding the thermal changes occurring in the HLS while the differential volumeters yield the associated volume changes undergone by the HLS during the pressure scans.

3. Main Results

A porous heterogeneous lyophobic system (HLS), also named repulsive clathrate (RC), is an ensemble of porous solid with large specific surface area (400 − 2000 m^2 g^{-1}) and corresponding non-wetting liquid,[4,9] which under certain conditions may have negative values of thermal expansion.[55] The condition of lyophobicity (contact angle between solid material and corresponding liquid $\theta > 90°$) does not allow for the liquid to spontaneously penetrate into the pores of the solid under ambient conditions (pressure and temperature). Forced intrusion of the liquid into the pores (say due to the increase of the pressure to some critical value P_{int}) decreases the volume of the HLS by the value of the pores volume of the lyophobic solid $\Delta V_{\text{int}} = -V_{\text{pores}}$. And the work stored in the system is

$$W_{\text{int}} = -P_{\text{int}}\Delta V_{\text{int}} = P_{\text{int}}V_{\text{pores}} \tag{1}$$

Since the presence of the non-wetting liquid inside the lyophobic pores is energetically unfavorable the process of liquid extrusion from the pores is spontaneous and occurs when the pressure is decreased to some critical value P_{ext}. If the liquid is fully expulsed from the pores, the HLS returns to its initial state $\Delta V_{\text{ext}} = V_{\text{pores}}$. The work restored by the system during the extrusion is

$$W_{\text{ext}} = -P_{\text{ext}}\Delta V_{\text{ext}} = -P_{\text{ext}}V_{\text{pores}} \tag{2}$$

In many cases[35] P_{int} and P_{ext} can be identified with Laplace capillary pressures:

$$P_{\text{int,ext}} = -\frac{\sigma\cos\theta_{\text{A,R}}}{kr_0} \tag{3}$$

Where the advancing contact angle θ_{A} is used for the intrusion pressure P_{int} and the receding contact angle θ_{R} is used for the extrusion pressure P_{ext}; σ is the surface tension of the liquid and k is a geometry parameter ($k = 0.5$ for cilinders and $k = 0.33$ for spheres), r_0 is an average pore radius. Applicability of eq. (3) is discussed in reference 35: for microporous materials, where the diameter of the pore is only of few molecular layers [4,8,25,26,43], such macroscopic parameter as the contact angle θ does not exist. However, for a mesoporous HLS the extrusion pressure is additionally determined by the condition of critical bubble nucleation inside the pores [56] and for both intrusion and extrusion pressures the effect of the line tension on the values of $\theta_{\text{A,R}}$ should be taken into account. [56]

Reversible intrusion/extrusion process is followed by the development/reduction of a large "solid – liquid" interface Ω development as:

$$\Delta V_{\text{int,ext}} = -kr\Delta\Omega \tag{4}$$

Hence if eq. (3) is applicable, the mechanical energy that HLS stores/restores during intrusion/extrusion process is determined by the Gibbs work of interface development/reduction:

$$\delta W_{\text{int,ext}} = -\sigma\cos\theta_{\text{A,R}}\,\mathrm{d}\Omega \tag{5}$$

Such development/reduction of the interface Ω is followed by an endothermal/exothermal effect (breakage/recovery of intermolecular bonds of the liquid), so during compression/ decompression a HLS also stores/restores thermal energy in the form of Gibbs heat of interface development/reduction:

$$\delta Q_{\text{int,ex}t} = T\frac{\mathrm{d}(\sigma\cos\theta_{\text{A,R}})}{\mathrm{d}T}\mathrm{d}\Omega \tag{6}$$

For a real HLS as described above the surface effects (which are dominant for a HLS) are always accompanied by classical bulk effects of the liquid and of the porous matrix. So the overall work and heat for HLS is defined as:

$$\begin{aligned}\delta W_{\text{c,d}} &= \delta W_{\text{int,ext}} + \delta W_0 \\ &= -\sigma\cos\theta_{\text{A,R}}\,\mathrm{d}\Omega + P\mathrm{d}V_0\end{aligned} \tag{7}$$

$$\begin{aligned}\delta Q_{\text{c,d}} &= \delta Q_{\text{int,ext}} + \delta Q_0 \\ &= T\frac{\mathrm{d}(\sigma\cos\theta_{\text{A,R}})}{\mathrm{d}T}\mathrm{d}\Omega + \delta Q_0\end{aligned} \tag{8}$$

Where indexes "c" and "d" stand for compression and decompression respectively, "0" indicates the bulk phase (liquid and matrix), $dV_0 = dV_L + dV_M$ determines change of the volume of the liquid V_L and of the matrix V_M due to pressure or temperature change. We have shown[35] that while the pressure

during intrusion/extrusion is determined by the Laplace eq.(3). The total volume change for HLS is;

$$dV_{c,d} = dV_{int,ext} + dV_0 \quad (9)$$

This volume being a function of pressure P and temperature T, one can develop a thermal equation of state for the HLS. [35] From this equation of state it is hence possible to derive the isobaric coefficient of the thermal expansion of the system $\alpha_{int,ext}$. The striking result was to demonstrate[35] that $\alpha_{int,ext}$ may become negative (effect of Negative Thermal Expansion, NTE).

As an example **Fig.3** shows the temperature dependence of α_{int} at $P = P_0 = 15$ MPa for the {WC8 + water} HLS obtained using such equation of state.

As can be seen from **Fig.3** the values of α for HLS may become negative in a certain temperature range, which indicates a negative thermal expansion. This effect takes place when the value of $P_{int}(T)$ gets closer to value of $P = P_0$ so that the intrusion provoked by the temperature increase occurs, which leads to the interface Ω development and the decrease of the volume of the HLS according to eq.(4). The calculated value of α reaches a maximum value of almost $-1.5 \cdot 10^{-3} K^{-1}$, which is more than an order of magnitude higher compared to best reported results.[6] Interestingly we have established [35] a simple method for determining the temperature range in which NTE occurs for a HLS.

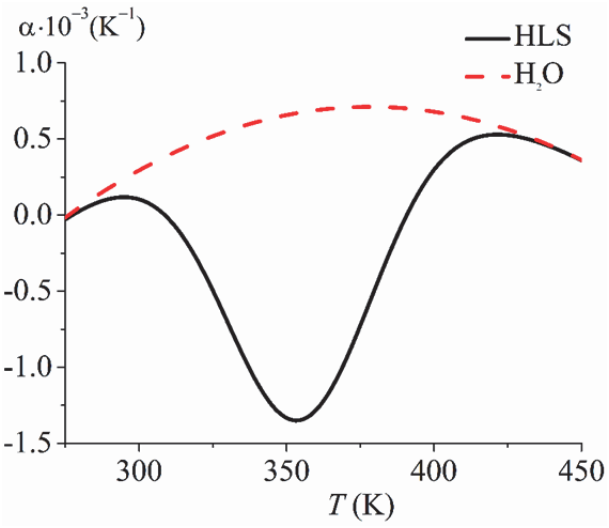

Fig.3 Isobaric coefficients of thermal expansion of the {WC8 + water} HLS [35] and of water [57] at 15 MPa.

At this point it is worth to investigate the stability of such MOF systems when they are utilized in a wide range of applications, particularly implying operations at very high pressures.

For this purpose two Zeolitic Imidazolate Frameworks (ZIFs) known for their high stability were selected: ZIF-67 and ZIF-8. In particular we have investigated [44] the concomitant effect of pressure and temperature upon water intrusion/ extrusion cycles. *P,V,T*-calorimetry is perfectly adapted to carry such systematic studies.

Taking the {ZIF-67 + water} system as an example successive intrusion–extrusion cycles were performed (with compression–decompression rate of 5.5 MPa min^{-1}) at different temperatures, see **Fig.4(a-c)**. One observes that each successive cycle provokes changes in *PV*-isotherms: decrease of both intrusion/extrusion pressures and intrusion/extrusion volume. Such changes lower the value of stored/restored energy per one compression–decompression cycle and this effect is much more pronounced at higher temperatures; at 275 K the stored/restored energy of the system decrease by about 20 % compared to the first cycle, at 330 K it is almost 100 %, while at 350 K there is no extrusion (no restored energy) after the first cycle. This result correlates with the degradation of the energetic characteristics of {ZIF-8 + water} system only at temperatures higher than 330 K as reported previously: water intrusion–extrusion cycles only at temperatures higher then *ca*. 330 K provoke irreversible changes in the structure of ZIF-8 and lowers its symmetry from cubic to orthorhombic. [7]

To better understand the reason for the {ZIF-67 + water} system's degradation further characterization methods like XRD and FTIR were performed. It appears that at temperatures higher than 330 K intrusion/extrusion cycles induce the formation of a new phase.[44] To focus on the degradation of the energetic characteristics of this system, additional intrusion–extrusion experiments were performed for this HLS under different dynamics (**Fig.4(d)**. First a new {ZIF-67 + water} sample was submitted to 5 intrusion–extrusion cycles after which it was kept in the measuring cell at atmospheric pressure for 3 days. Remarkably, after this long pause the 6th compression–decompression cycle demonstrates the recoverability [58] of the energetic characteristics of the system (**Fig.4(d)**): the intrusion pressure is equal to intrusion pressure at the first cycle, while extrusion pressure and volume of intruded water correspond to those of the a second cycle (even for most stable HLSs, which undergo millions of cycles it is typical that the first cycle is different from all following ones. [15,17]

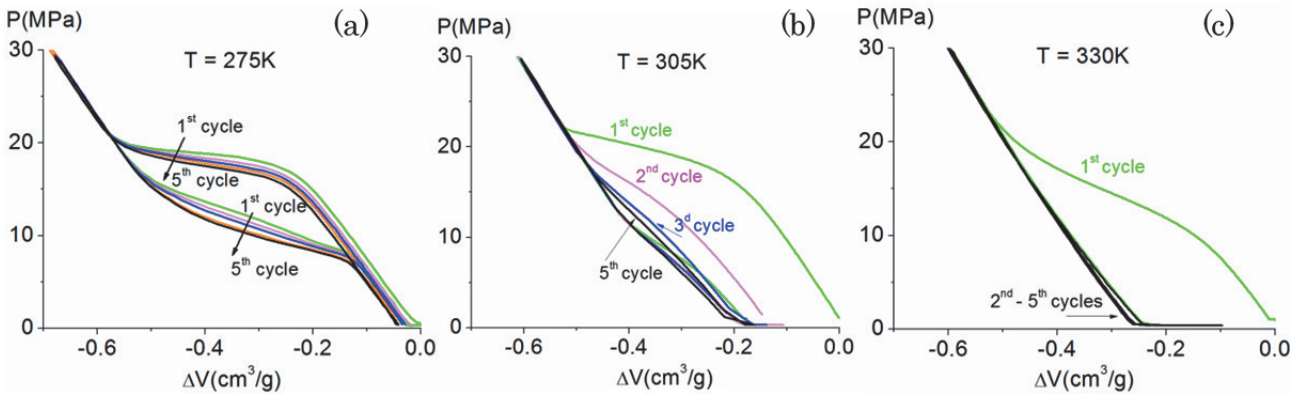

Fig.4(a-c) *PV*-isotherms of {ZIF-67 + water} system, effect of temperature. [44]

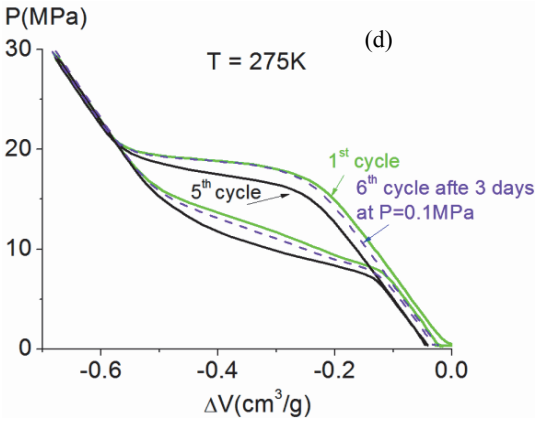

Fig.4(d) Effect of pause after successive cycling. [44]

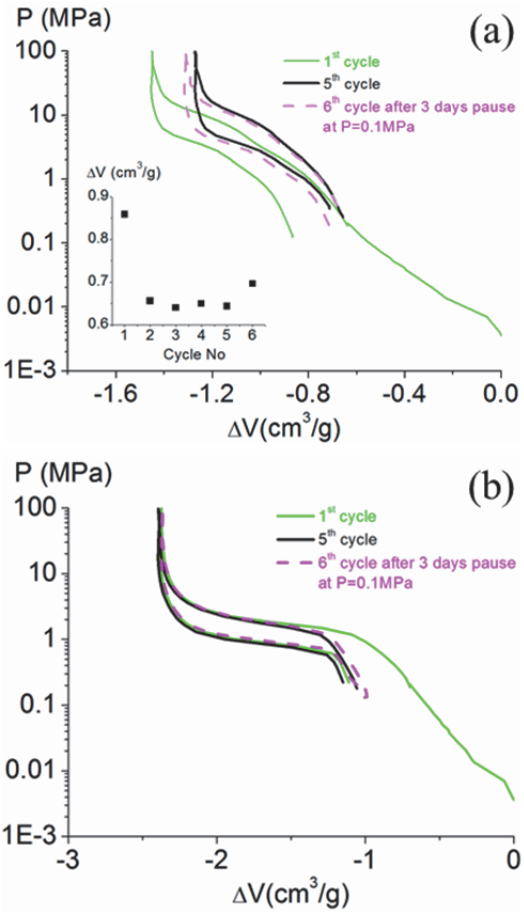

Fig.5 Compression / Decompression isotherms of (a) {ZIF-67+mercury} and (b) {ZIF-8+mercury} systems. [44]

In fact such experiments were previously proposed to study the huge flexibility of MIL-53 MOF for mechanical energy applications.[58] We followed this approach and performed compression–decompression cycles of {ZIF-67 + mercury} system in the 0.004–100 MPa pressure range for investigating the flexibility of ZIF-67 and ZIF-8. High surface tension of mercury prevents its intrusion into the micropores of these ZIFs. **Fig.5(a)** shows that at the pressure of *ca*. 5 MPa, ZIF-67 undergoes pronounced volume variation associated with the flexibility of its framework. The volume variation due to such flexible effect decreases after the first compression–decompression cycle, but tends to recover at the 6th cycle after 3 days pause.

This result complies well with intrusion–extrusion experiments at 275 K (**Fig.4(d)**) and suggests that the observed slow relaxation of energetic characteristics of {ZIF- 67 + water} system is due to the relaxation of the flexible ZIF-67 framework. It also can be seen that for ZIF-67 framework the flexibility takes place in two steps. Most likely, this explains the two-step water extrusion of {ZIF-67 + water} system (**Fig.4**). In recent work it was experimentally shown that the threshold pressure at which reversible flexibility effect of MOF occurs depends on the pressurizing fluid.[32] This explains the fact that there is no observable flexibility effect at about 5 MPa before water intrusion (**Fig.4**). From these experiments we see that 3 times lower pressure impact upon water intrusion (**Fig.4(b)**) has much more prominent effect on ZIF-67 compared to 100 MPa impact under non-intrusion conditions (**Fig.5(a)**).

Such results are worth to compare with the pressure induced flexibility effect of ZIF-8 in **Fig.5(b)** This MOF exhibits much lower pressure of about 2 MPa with almost negligible decrease of the *breathing effect* (that is the *framework relaxation* due to the framework flexibility) inducing the volume variation at each successive cycle and fast recovery of about 30 min. However, it is possible to detect some differences on *PV*-isotherms of the {ZIF-8 + water} system depending on the speed of compression–decompression cycle using the more sensitive to volume variations Transitiometer ST-7M (**Fig.6**): one observes that for all the investigated regimes the intrusion process is a one-step process associated with one-step plateau on the *PV*-isotherm due to forced intrusion of water molecules into the pores of ZIF-8. For extrusion it is a two-step process, which is well seen on the derivative plot in the inserts of **Fig.6** (two peaks of compressibility for extrusion, with only one peak

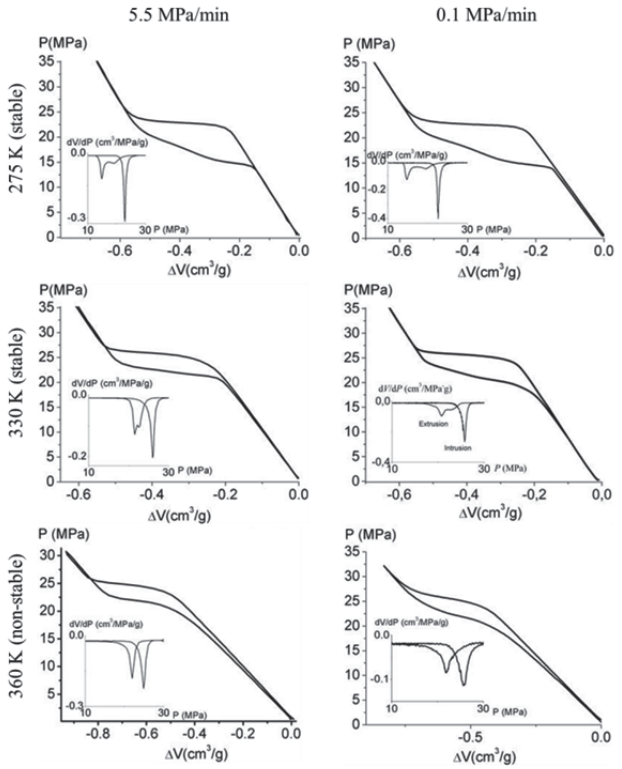

Fig.6 *PV*-isotherms and compressibilities (inserts) of {ZIF-8 + water} system at three different temperatures (275,330, and 360 K), and for two compression-decompression rates (5.5 MPa min^{-1} and 0.1 MPa min^{-1} respectively). [44]

Table 1 Energetic characteristics of ZIFs based systems upon compression-decompression cycle: E_{st} and E_{rst} are stored and restored energies, H is stored-restored energy hysteresis, P_C is threshold pressure upon compression, P_D is threshold pressure upon decompression, ΔV is volume variation.

System	T, K	E_{st}, J g^{-1}	E_{rst}, J g^{-1}	H, %	P_C, MPa	P_D, MPa	ΔV, cm^3 g^{-1}
{ZIF-67 + water}	275	6.6	4.1	38	18.8	11.6	0.35
{ZIF-8 + water}	275	8.8	5.7	35	23.0	17.3	0.43
{ZIF-67 + mercury}	295	2.5	1.0	60	10.0	4.0	0.25
{ZIF-8 + mercury}	295	1.9	0.9	53	1.8	0.8	1.07

for intrusion). One observes also that the two-step extrusion process shifts to one-step extrusion process as both temperature and compression–decompression speed increases. Considering the experiments described above, it appears that the slow kinetics of the breathing of ZIF-8 structure is the reason for the two-step extrusion and the threshold pressure of breathing effect might be temperature dependent. The energetic characteristics of ZIF-67 and ZIF-8 obtained upon water intrusion–extrusion and the flexibility effect are listed together in **Table 1**: the {ZIF-8 + water} system has the best energetic indexes and is proven to be stable under high pressure in the 275 – 330 K temperature range. [7)]

4. Concluding Remarks

This short review is essentially based on some of our most recent contributions on the surface energy developed by porous Heterogeneous Lyophobic Systems (HLS). It shows that HLSs systems may exhibit pronounced negative thermal expansion (NTE). It also reports investigation of the stability of MOF ZIF-67 under high-pressure water intrusion cycles which reveals that MOF ZIF-67 stability in these conditions is highly temperature dependent. Such results present similarity with the stability of MOF ZIF-8 and may provide powerful tests of MOFs' stability, that is: the impact of temperature and pressure to be investigated not only separately, but also concomitantly. In this respect we demonstrate the power of *P,V,T*-calorimetry, particularly in its version scanning transitiometry coupled to volumetry to perform original in depth investigations of such heterogeneous systems.

In addition we give a documented approach of the pronounced breathing effect of ZIF-67 and ZIF-8 MOFs under compression–decompression cycles at rather low pressure, which can be used for mechanical energy storage following previously suggested applications.[59)] Finally, the effect of compression–decompression speed on the {ZIF-8 + water} system is shown to take place even in a rather narrow pressure range, which means that such systems must be tested also at much higher operational frequencies to be used for practical engineering developments.

References

1) A. Y. Fadeev and V. Eroshenko, *J. Colloid Interface Sci*. **187**, 275−282 (1997).
2) J. Rouquerol, G. Baron, R. Denoyel, H. Giesche, J. Groen, P. Klobes, P. Levitz, A. V. Neimark, S. Rigby, R. Skudas, K. Sing, M. Thommes, and K. Unger, (IUPAC Technical Report) *Pure Appl. Chem*. **84**, 107−136 (2012).
3) N. Cavazzini, L. Marchetti, R. Pasti, F. Greco, A. Dondi, A. Laganà, A. Ciogli, and F. Gasparrini, *Anal. Chem*. **85**, 19−22 (2013).
4) V. Eroshenko, R. C Regis, M. Soulard, and J. Patarin, *J. Am. Chem. Soc.* **123**, 8129−8130 (2001).
5) L. Tzanis, M. Trzpit, M. Soulard, and J. Patarin, *J. Phys. Chem. C*. **116**, 4802–4808 (2012).
6) A. V. Erochenko, *Proc. Inst. Mech. Eng., Part D, J. Automob. Eng*. **221**, 285−300 (2007); V. D. Borman, A. A. Belogorlov, and V. N. Tronin, *arXiv preprint arWiv*, 1505.05476 (2015).
7) Y. Grosu, G. Renaudin, V. Eroshenko, J.-M. Nedelec, and J.-P. E. Grolier, *Nanoscale* **7**, 8803-8810 (2015).
8) O. V. Ievtushenko, V. A. Eroshenko, Y. G. Grosu, J. M. Nedelec, and J.P. E. Grolier, *Phys. Chem. Chem. Phys.* **15**, 4451−4457 (2013).
9) V. A. Eroshenko, *Soviet Patent* No. 1,254,811, 1981, [priority of 24.07.1981, updated 02.09.1993 (date of free public access)].
10) V. Eroshenko, R. C. Regis, M. Soulard, and J. Patarin, *C. R. Phys*. **3**, 111−119 (2002).
11) Y. Qiao, V. K. Punyamurtula, A. Han, X. Kong, and F.B. Surani, *Appl. Phy. Lett.* **89**, 251905−251908 (2006).
12) O.V. Ievtushenko, V.A. Eroshenko, Y.G. Grosu, J.-M. Nedelec, and J-P. E. Grolier, *Phys. Chem. Chem. Phys.* **15**, 4451−4457 (2013).
13) V. A. Eroshenko, *Patent* 94/14856, 1 (1994).
14) V. A. Eroshenko, *Patent WO* 01/55616, A1 (2001).
15) C. V. Suciu, T. Iwatsubo, and S. Deki, *J. Colloid Interface Sci*. **259**, 62−80 (2003).
16) A. V. Erochenko, I. Piatiletov, L. Coiffard, and V. Stoudenets, *Proc. Inst. Mech. Eng., Part D, J. Automob. Eng*. **221**, 301−312 (2007).
17) C. V. Suciu and K. Yaguchi, *Exp. Mech. Int. J.* **49**, 383−393 (2009).
18) C. V. Suciu, S. Tani, and K. Miyoshi, *J. Syst. Des. Dyn.* **4**, 899−913 (2010).
19) L. Guillemot, *Ph. D. Thesis. Institut National des Sciences Appliquées*, Lyon, France (2010).
20) C. V. Suciu, I. Iwatsubo, K. Yaguchi, and M. Ikenaga, *J. Colloid Interface Sci*., **283**, 196−214 (2005).
21) T. Karbowiak, M. A. Saada, S. Rigolet, A. Ballandras, G. Weber, I. Bezverkhyy, M. Soulard, J. Patarin, and J. P. Bellat, *Phys. Chem. Chem. Phys*. **12**, 11454−11466 (2010).
22) Y. Qiao and A. Han, *Philos. Mag. Lett.* **87**, 25-31 (2007).
23) A. Han, W. Lu, T. Kim, X. Chen, and Y. Qiao, *Phys. Rev. E* **78**, 031408 (2008).
24) L. Coiffard, V. A. Eroshenko, and J. P. E. Grolier, *AIChE J.* **51**, 1246−1257 (2005).
25) G. Ortiz, H. Nouali, C. Marichal, G. Chaplais, and J. Patarin, *Phys. Chem. Chem. Phys*. **15**, 4888−4891 (2013).
26) L. Tzanis, M. Trzpit, M. Soulard, and J. Patarin, *J. Phys. Chem. C* **116**, 20389−20395 (2014).
27) J. Canivet, A. Fateeva, Y. Guo, B. Coasne, and D. Farrusseng, *Chem. Soc. Rev*. **43**, 5594−5617 (2014).
28) U. Mueller, M. Schubert, F. Teich, H. Puetter, K. Schierle-Arndt, and J. Pastre, *J. Mater. Chem.* **16**, 626−6360 (2006).
29) J. R. Li, R. J. Kuppler, and H. C. Zhou, *Chem. Soc. Rev*. **38**, 1477−1504 (2009).
30) D. Farrusseng, in *Metal–organic frameworks: applications from catalysis to gas storage*, Wiley (2011).
31) P. Horcajada, C. Serre, G. Maurin, N. A. Ramsahye, F. Balas, M. Vallet-Regí, M. Sebban, F. Taulelle, and G. Férey,

J. Am. Chem. Soc. **130**, 6774−6780 (2008); P. Horcajada, T. Chalati, C. Serre, B. Gillet, C. Sebue, T. Baati, J. F. Eubank, D. Heurtaux, P. Clayette, C. Kreuz, J.S. Chang, Y. K. Hwang, V. Marsaud, P. N. Bories, L. Cynder, S. Gil, G. Frérey, P. Couvreur, and R. Gref, *Nat. Mater*. **9**, 172−178 (2010).
32) J. Rodriguez, I. Beurroies, T. Loiseau, R. Denoyel, and P. L. Llewellyn, *Angew. Chem., Int. Ed.* **54**, 4626−4630 (2015).
33) G. Ortiz, H. Nouali, C. Marichal, G. Chaplais, and J. Patarin, *J. Phys. Chem. C* **118**, 5397−5405 (2014). M. Michelin-Jamois, C. Picard, E. Charlaix, and G. Vigier, *arXiv preprint rXiv*:1404.5318 (2014).
34) G. Ortiz, H. Nouali, C. Marichal, G. Chaplais, and J. Patarin, *J. Phys. Chem. C* **118**, 7321−7328 (2014).
35) V. A. Eroshenko, Y.Grosu, N. Tsyrin, V. Stoudenets, J-M. Nedelec, and J-P. E. Grolier, *J. Phys. Chem. C.* **119**, 10266−10272 (2015).
36) K. W. Chapman, G. J. Halder, and P. J. Chupas, *J. Am. Chem. Soc*. **131**, 17546−17547 (2009).
37) S. A. Moggach, T. D. Bennett, and A. K. Cheetham, *Angew. Chem., Int. Ed*. **121**, 7221−7223 (2009).
38) T. D. Bennett, P. Simoncic, S. A. Moggach, F. Gozzo, P. Macchi, D. A. Keen, J.-C. Tan, and A. K. Cheetham, *Chem. Commun*. **47**, 7983−7985 (2011).
39) K. S. Park, Z. Ni, A. P. Côté, J. Y. Choi, R. Huang, F. J. Uribe-Romo, H. K. Chae, M. O'Keeffe, and O. M. Yaghi, *Proc. Natl.Acad. Sci.* **103**, 10186−10191 (2006).
40) Z. Hu, L. Zhang, and J. Jiang, *J. Chem. Phys*. **136**, 244703 (2012).
41) A. U. Ortiz, A. Boutin, A. H. Fuchs, and F. X. Coudert, *J. Phys. Chem. Lett*. **4**, 1861−1865 (2013).
42) Y. Hu, H. Kazemian, S. Rohani, Y. Huang, and Y. Song, *Chem. Commun*. **47**, 12694−12696 (2011).
43) Y. Grosu, V. Eroshenko, J.-M. Nedelec, and J.-P. E. Grolier, *Phys. Chem. Chem. Phys*. **17**, 1572−1574 (2015).
44) Y. Grosu, S. Gomes, G. Renaudin, J-P. E. Grolier, V. Eroshenko, and J-M. Nedelec, *RSC Advances* **5**, 89498−89502 (2015).
45) Y. Pan, Y. Liu, G. Zeng, L. Zhao, and Z. Lai, *Chem. Commun*. **47**, 2071−2073 (2011).
46) J. Qian, F. Sun, and L. Quin, *Mater. Lett*. **82**, 220−223 (2012).
47) R. Banerjee, A. Phan, B. Wang, C. Knobler, H. Furukawa, M. O'Keeffe, and O.M. Yaghi, *Science* **319**, 939−943 (2008).
48) M. Michelin-Jamois, L. Guillemot, T. Abensur, E. Charlaix, and G. Vigier, *Proceedings of the 5th European Conference for Aeronautics and Space Sciences*, Munich, Germany (2013).
49) L. Coiffard, and V. Eroshenko, *J. Colloid Interface Sci*. **300**, 304–309 (2006).
50) S. L. Randzio, J.-P. E. Grolier, J. Zaslona, and J. R. Quint, *French Patent* No. 9109227, (1994); *Polish Patent No*. 295285, (1995).
51) S. L. Randzio, *Chem. Soc. Rev.*, **25**, 383−392 (1996).
52) S. L. Randzio, and J.-P. E. Grolier, *Anal. Chem*. **70,** 2327−2330 (1998).
53) S. L. Randzio, Ch. Stachowiak, and J-P. E. Grolier, *J. Chem. Thermodyn.* **35**, 639−648 (2003).
54) D. S. Nyce, in *Linear Position Sensors: Theory and Application*, Wiley-Interscience, New Jersey, (2004).
55) V. A. Eroshenko, (in Russian). *Ind.Heat Eng*. **1−3**, 22−25 (1992); Y. Grosu, V. Eroshenko, O. Ievtushenko, J-M. Nedelec, and J-P. E. Grolier, *Ukr. J. Phys*. **59**, 69−78 (2014).
56) Y. Grosu, O. Ievtushenko, V. Ereoshenko, J-M. Nedelec, and J-P. E. Grolier, *Colloids Surf. A: Phys. Chem. Eng. Asp.* **441**, 549−555 (2014).
57) NIST Chemistry, WebBook. *Webbook.nist. gov/chemistry*.
58) A. Rebello, J. J. Neumeier, Z. Gao, and Y. Ma, *Phys. Rev. B* **86**, 104303−104309 (2012).
59) I. Beurrois, M. Boulhout, P. L. Llewellyn, B. Kuchta, G. Frérey, C. Serra, and R. Denoyel, *Angew. Chem. Int. Ed.* **49**, 7526−7529 (2010).